V European Conference on Computational Fluid Dynamics
ECCOMAS CFD 2010
J. C. F. Pereira and A. Sequeira (Eds)
Lisbon, Portugal, 14–17 June 2010

STRESS-STRAIN ANALYSIS IN THE STOMACH

R. N. Miftahof

College of Medicine and Medical Sciences, Arabian Gulf University
Manama, Kingdom of Bahrain
roustem@agu.bh

Key words: Stomach, Mathematical model, Stress-strain analysis

Abstract. *A biomechanical model of the human stomach is proposed. The process of electromechanical conjugation and the spread of the electromechanical wave along the stomach wall were analyzed numerically. Results revealed patterns of stress-strain distribution in the organ. The circular smooth muscle layer produced greater total forces throughout in comparison to the outer longitudinal smooth muscle layer. The body of the organ along the lesser curvature and the cardia-fundus areas were overstressed compare to other regions. There is currently no affirmative experimental evidence to provide a detailed quantitative comparison of the results.*

1 INTRODUCTION

Mathematical modeling allows one to gain the insight into hidden physiological mechanisms of function of experimentally inaccessible abdominal viscera [1-7]. However, most of the proposed models are based on a reductionist "mechanistic" approach and, therefore, have a limited biological plausibility. Furthermore, these studies have been hampered by indiscrete and often inappropriate applications of ideas and methods borrowed from the mechanics of shells to describe their biomechanical behavior. It should be emphasized that biomechanics is not just the transformation of general laws and principles of mechanics to the study of biological phenomena, but rather the adequate development and extension of these laws and principles to the modeling and analysis of living things.

The aims of this study are: i) to formulate a biomechanical model of the human stomach as a thin soft biological shell, and ii) to study the dynamics of the propagation of electromechanical waves within the organ under normal physiological conditions.

2 PHYSIOLOGICAL REMARKS

The configuration of the stomach is determined by: i) the amount of the content, ii) the stage of the digestive process, iii) the degree of development of the gastric musculature, and iv) the condition of the adjacent loops of the small and large intestines. Physiological responses of the stomach to internal and external stimuli depend entirely on the inherent activity of histomorphological elements: smooth muscle cells, neurons, interstitial cells of Cajal, and their topographical organization in gastric tissue [8-10]. Longitudinal and circular smooth muscle layers are formed of smooth muscle cells are embedded into a network of collagenous and elastin fibers and are coupled via gap junctions into three distinct syncytia (muscle layers).

The smooth muscle syncytia react with a variety of rhythmical movements which are a result of an electrochemical coupling phenomenon. Electrophysiological and molecular cloning studies have shown that L - and T - type Ca^{2+} channels, Ca^{2+} - K^{+}, selective K^{+}, Na^{+}, leak Cl^{-}, and nonselective cation channels are responsible for electrical activity of smooth muscle syncytia represented by slow waves and spikes [11,12].

Connective tissue elastin and collagen fibers are built in a three dimensional loosely woven network. Elastin may be stretched to 250% of the unloaded configuration. Collagen is relatively inextensible stiff reinforcing structural component, and the main load carrying element. Collagen fibers are usually undulated and they become stiff when straightened under the action of applied loads. The strength of tissues is strongly correlated with the collagen content.

Motility signals in the stomach originate in the upper part of the body of the organ. Three types of mechanical waves are observed: i) small isolated contraction waves, ii) peristaltic waves that slowly move from the point of origin down toward the pyloric sphincter, and iii) nonpropagating waves.

3 MECHANICAL PROPERTIES

The soft tissue that makes the wall of the stomach is characterized as transversely anisotropic nonhomogenous viscoelastic biocomposite that undergoes finite strains. This has been convincingly demonstrated in quasistatic uniaxial tests on specimens collected from different regions of the organ [13]. Experiments under biaxial tension have shown that the shear force applied to the tissue is significantly less, $0.01T_{\max}$, compared with the tangential force [14].

The complex behavior of the stomach has also been studied under complex loading, i.e., a combined inflation with subsequent external local compression of the anterior surface of the organ [15]. Instantaneous intraluminal pressure, volume and stress-strain recordings indicate that in the low pressure domain $0.1 \le P \le 3.0$ (kPa) the stomach experiences biaxial stress-strain states and smooth continuous deformations in all regions. In the higher pressure range $3.0 < P \le 25$ (kPa) creases appear in the cardia-fundal and antrum-pyloric areas.

4 MATHEMATICAL MODEL

Let every point of the middle surface of the undeformed stomach be referred to the global Cartesian coordinate system x, y, z. Assume that the organ is inflated by intraluminal pressure p and subsequently excited by electrical discharges of the pacemaker cell of a given intensity and duration. As a result of depolarization the electrical waves are produced in the longitudinal and circular smooth muscle syncytia. They propagate along the surface of the organ and generate active forces of contraction-relaxation.

Mathematical formulation of the problem of the dynamics of electromechanical wave activity in the stomach comprises the equations of motion of the thin soft shell, constitutive relations for mechanical and cable electrical properties of the biocomposite, initial and boundary conditions. The equations of motion of the soft biological shell are given by

$$\rho_0 \frac{\partial v_x}{\partial t} = \frac{\partial}{\partial \tilde{s}_1}\left[\left(k\frac{\partial(\lambda_c - 1)}{\partial t} + T^a(\lambda_c) + T^p(\lambda_c, \lambda_l)\right) e_{1x}\sqrt{a_{22}}\right] + \frac{\partial}{\partial \tilde{s}_2}\left[\left(k\frac{\partial(\lambda_l - 1)}{\partial t} + T^a(\lambda_l) + T^p(\lambda_c, \lambda_l)\right) e_{2x}\sqrt{a_{11}}\right] + p\sqrt{a}\,\bar{n}_x,$$

$$\rho_0 \frac{\partial v_y}{\partial t} = \frac{\partial}{\partial \tilde{s}_1}\left[\left(k\frac{\partial(\lambda_c - 1)}{\partial t} + T^a(\lambda_c) + T^p(\lambda_c, \lambda_l)\right) e_{1y}\sqrt{a_{22}}\right] + \frac{\partial}{\partial \tilde{s}_2}\left[\left(k\frac{\partial(\lambda_l - 1)}{\partial t} + T^a(\lambda_l) + T^p(\lambda_c, \lambda_l)\right) e_{2y}\sqrt{a_{11}}\right] + p\sqrt{a}\,\bar{n}_y, \tag{1}$$

$$\rho_0 \frac{\partial v_z}{\partial t} = \frac{\partial}{\partial \tilde{s}_1}\left[\left(k\frac{\partial(\lambda_c - 1)}{\partial t} + T^a(\lambda_c) + T^p(\lambda_c, \lambda_l)\right) e_{1z}\sqrt{a_{22}}\right] + \frac{\partial}{\partial \tilde{s}_2}\left[\left(k\frac{\partial(\lambda_l - 1)}{\partial t} + T^a(\lambda_l) + T^p(\lambda_c, \lambda_l)\right) e_{2z}\sqrt{a_{11}}\right] + p\sqrt{a}\,\bar{n}_z,$$

where $\tilde{s}_1, \tilde{s}_2$ are the Lagrangian curvilinear orthogonal coordinates and t is time. The components of the velocity vector v_x, v_y and v_z are

$$v_x = \frac{dx}{dt}, v_y = \frac{dy}{dt}, v_z = \frac{dz}{dt}. \tag{2}$$

The rate of elongation (hereafter, the subscripts (l) and (c) are referred to the longitudinal and circular muscle layers, respectively), are calculated as

$$\lambda_c = \frac{dx}{d\overset{\circ}{\tilde{s}}_1}, \lambda_l = \frac{dy}{d\overset{\circ}{\tilde{s}}_2}. \tag{3}$$

The components and the determinant of the metric tensor are defined by

$$a_{ij} = \frac{\partial x}{\partial \tilde{s}_i}\frac{\partial x}{\partial \tilde{s}_j} + \frac{\partial y}{\partial \tilde{s}_i}\frac{\partial y}{\partial \tilde{s}_j} + \frac{\partial z}{\partial \tilde{s}_i}\frac{\partial z}{\partial \tilde{s}_j}$$

$$a = a_{11}a_{22} - a_{12}^2 \qquad (i = 1,2) \tag{4}$$

and the cosines of the outward normal $\bar{n}$ to the surface with respect to the x, y, z axes are calculated as

$$e_{ix} = \frac{1}{\sqrt{a_{ii}}}\frac{\partial x}{\partial \tilde{s}_i}, \quad e_{iy} = \frac{1}{\sqrt{a_{ii}}}\frac{\partial y}{\partial \tilde{s}_i}, \quad e_{iz} = \frac{1}{\sqrt{a_{ii}}}\frac{\partial z}{\partial \tilde{s}_i},$$

$$\begin{aligned} \bar{n}_x &= (e_{1y}e_{2y} - e_{1z}e_{2z})\sqrt{a_{11}a_{22}}/\sqrt{a}, \\ \bar{n}_y &= (e_{1z}e_{2x} - e_{1x}e_{2s})\sqrt{a_{11}a_{22}}/\sqrt{a}, \\ \bar{n}_z &= (e_{1x}e_{2y} - e_{1y}e_{2x})\sqrt{a_{11}a_{22}}/\sqrt{a}. \end{aligned} \tag{5}$$

The passive $T_{c,l}^p$ and active $T_{c,l}^a$ forces of the total membrane force are given by

$$T_{c,l}^p = \frac{\partial \rho_0 W}{\partial(\lambda_{c,l} - 1)}, \tag{6}$$

$$T_{c,l}^a = \begin{cases} 0, & [Ca^{2+}] \le 0.1\ \mu M \\ c_7 + c_8[Ca^{2+}]^4 + c_9[Ca^{2+}]^3 + c_{10}[Ca^{2+}]^2 + c_{11}[Ca^{2+}], & 0.1 < [Ca^{2+}] \le 1\mu M \\ \max T^a, & [Ca^{2+}] > 1\mu M \end{cases}, \tag{7}$$

where W is the strain energy density function of the connective tissue network and passive muscle tissue

$$\rho_0 W = \frac{1}{2}\Big[c_1(\lambda_l - 1)^2 + 2c_3(\lambda_l - 1)(\lambda_c - 1) + c_2(\lambda_c - 1)^2 + \\ + c_{14}\exp\Big(c_4(\lambda_l - 1)^2 + c_5(\lambda_c - 1)^2 + 2c_6(\lambda_l - 1)(\lambda_c - 1)\Big)\Big].$$

Here $c_{1\text{-}11}$ are empirically defined mechanical constants, and $[Ca^{2+}]$ is the concentration of free intracellular calcium.

Changes in the free cytosolic calcium concentration yield

$$d[Ca^{2+}]/dt = 0.2z(\varphi_{Ca} - \varphi_{(c,l)})/(1 + \zeta[Ca^{2+}]) - 0.3[Ca^{2+}]. \tag{8}$$

Here φ_{Ca} is the reversal potential for the calcium ion current; ζ is the parameter of inhibition of the Ca^{2+} channels; z is the dynamic variable of the ionic channels whose kinetics is given by

$$\frac{dz}{dt} = \left(\frac{1}{1+\exp(-\,0.15(\varphi_{(c,l)} + \,42)} - z \right) / \tau_z \,, \tag{9}$$

τ_z is the time constant.

The dynamics of the propagation of the electrical wave, φ_l, along the anisotropic longitudinal muscle layer is given by

$$C_m \frac{\partial \varphi_l}{\partial t} = I_{m1}(\tilde{s}_1, \tilde{s}_2) + I_{m2}(\tilde{s}_1 - \tilde{s}'_1, \tilde{s}_2 - \tilde{s}'_2) + I^*_{ionic}, \tag{10}$$

where I_{m1}, I_{m2} are the transmembrane currents

$$\begin{aligned} I_{m1}(\tilde{s}_1, \tilde{s}_2) = M_{vs} \Bigg\{ & -\frac{2(\mu_{\tilde{s}_1} - \mu_{\tilde{s}_2})}{(1+\mu_{\tilde{s}_1})(1+\mu_{\tilde{s}_1})} \arctan\left(\frac{d\tilde{s}_1}{d\tilde{s}_2} \sqrt{\frac{G_{\tilde{s}_2}}{G_{\tilde{s}_1}}} \right) + \\ & + \frac{g^*_{0,\tilde{s}_2}}{G_{\tilde{s}_1}} \Bigg\} \left(\frac{\partial}{\partial \tilde{s}_1} \left(\frac{g^*_{0,\tilde{s}_1}}{\lambda_c} \frac{\partial \varphi_l}{\partial \tilde{s}_1} \right) + \frac{\partial}{\partial \tilde{s}_2} \left(\frac{g^*_{0,\tilde{s}_2}}{\lambda_l} \frac{\partial \varphi_l}{\partial \tilde{s}_2} \right) \right), \end{aligned}$$

$$\begin{aligned} I_{m2}(\tilde{s}_1, \tilde{s}_2) = M_{vs} \iint_S & \frac{\mu_{\tilde{s}_1} - \mu_{\tilde{s}_2}}{2\pi(1+\mu_{\tilde{s}_1})(1+\mu_{\tilde{s}_1})} \frac{(\tilde{s}_2 - \tilde{s}'_2)/G_{\tilde{s}_2} - (\tilde{s}_1 - \tilde{s}'_1)/G_{\tilde{s}_1}}{\left[(\tilde{s}_1 - \tilde{s}'_1)/G_{\tilde{s}_1} - (\tilde{s}_2 - \tilde{s}'_2)/G_{\tilde{s}_2} \right]^2} \\ & \times \left(\frac{\partial}{\partial \tilde{s}_1} \left(\frac{g^*_{0,\tilde{s}_1}}{\lambda_c} \frac{\partial \varphi_l}{\partial \tilde{s}_1} \right) + \frac{\partial}{\partial \tilde{s}_2} \left(\frac{g^*_{0,\tilde{s}_2}}{\lambda_l} \frac{\partial \varphi_l}{\partial \tilde{s}_2} \right) \right) d\tilde{s}'_1 \, d\tilde{s}'_2, \end{aligned} \tag{11}$$

$$\mu_{\tilde{s}_1} = g^*_{0,\tilde{s}_1} / g^*_{i,\tilde{s}_1}, \quad \mu_{\tilde{s}_2} = g^*_{0,\tilde{s}_2} / g^*_{i,\tilde{s}_2},$$

$$G_{\tilde{s}_1} = \frac{g^*_{0,\tilde{s}_1} + g^*_{i,\tilde{s}_1}}{\lambda_c}, \; G_{\tilde{s}_2} = \frac{g^*_{0,\tilde{s}_2} + g^*_{i,\tilde{s}_2}}{\lambda_l}, \; G = \sqrt{G_{\tilde{s}_1} G_{\tilde{s}_2}} \,.$$

Here C_m is the capacitance of smooth muscle; $g^*_{i,\tilde{s}_1}$, $g^*_{i,\tilde{s}_2}$, $g^*_{0,\tilde{s}_1}$, $g^*_{0,\tilde{s}_2}$ are the maximal intracellular (i) and interstitial space (0) conductivities of the longitudinal and circular muscle layers; M_{vs} is the membrane volume-to-surface ratio. The total ion current, I^*_{ionic}, is defined as

$$I^*_{ionic} = \bar{g}_{Na} m^{*3} h^* (\varphi_{(c,l)} - \bar{\varphi}_{Na}) + \bar{g}_K n^{*4} (\varphi_{(c,l)} - \bar{\varphi}_K) + \bar{g}_\theta (\varphi_{(c,l)} - \bar{\varphi}_\theta) \,, \tag{12}$$

where $\bar{g}_{Na}$, $\bar{g}_K$, $\bar{g}_\theta$ are the maximal conductances and $\bar{\varphi}_{\mathrm{Na}}$, $\bar{\varphi}_{\mathrm{K}}$, $\bar{\varphi}_\theta$ are the reversal potentials of Na^+, K^+, and Cl^- currents. The dynamics of change in the probability variables m^*, h^*, and n^* of opening of the ion gates are obtained from the solution of the first-order equation

$$\frac{d\eta}{dt} = \alpha^*_\eta (1 - \eta) - \beta^*_\eta \eta, \qquad (\eta = m^*, h^*, n^*)$$

The activation, α^*_η, and deactivation, β^*_η, parameters satisfy the empirical relations

$$
\begin{aligned}
\alpha_m^* &= 0.005(\varphi_{(c,l)} - \overline{\varphi}_m) / [\exp 0.1(\varphi_{(c,l)} - \overline{\varphi}_m) - 1], \\
\beta_m^* &= 0.2 \exp(\varphi_{(c,l)} + \overline{\varphi}_m) / 38, \\
\alpha_h^* &= 0.014 \exp[-(\overline{\varphi}_h + \varphi_{(c,l)}) / 20], \\
\beta_h^* &= 0.2 / [1 + \exp 0.2(\overline{\varphi}_h - \varphi_{(c,l)})], \\
\alpha_n^* &= 0.006(\varphi_{(c,l)} - \overline{\varphi}_n) / [\exp 0.1(\varphi_{(c,l)} - \overline{\varphi}_n) - 1], \\
\beta_n^* &= 0.75 \exp(\overline{\varphi}_n - \varphi_{(c,l)}).
\end{aligned}
\tag{13}
$$

The dynamics of the propagation of the electrical wave, φ_c, along the isotropic circular smooth muscle syncytium is given by

$$
C_m \frac{\partial \varphi_c}{\partial t} = \frac{M_{vs}}{1 + \mu_{\tilde{s}_1}} \left\{ \frac{\partial}{\partial \tilde{s}_1} \left(\frac{g^*_{0,\tilde{s}_1}}{\lambda_c} \frac{\partial \varphi_c}{\partial \tilde{s}_1} \right) + \frac{\partial}{\partial \tilde{s}_2} \left(\frac{g^*_{0,\tilde{s}_1}}{\lambda_l} \frac{\partial \varphi_c}{\partial \tilde{s}_2} \right) \right\} - I^*_{ionic}, \tag{14}
$$

where the above-mentioned abbreviations and relationships for I^*_{ionic}, equations (10-12), are used.

The gastric pressure, p, changes according to the adiabatic law

$$
p = p_0 \Delta V^{1.41}, \tag{15}
$$

here p_0 is the meaning of p at $t = 0$; $\Delta V = V_0/V$ is the ratio of a current intraluminal volume, V, to its initial value, V_0.

The cardiac and pyloric ends of the organ are clamped. The initial conditions assume that the stomach is in the resting state. Excitation to the system is provided by electrical discharges of the pacemaker cell that are modeled as an input impulse of a given amplitude, φ_0, and duration t_d.

The combined nonlinear system of partial and ordinary differential equations (1)-(15) was solved numerically. Hybrid finite difference and finite element methods of second order accuracy, with respect to spatial and time variables, were employed.

5 RESULTS

5.1 Inflated stomach

Consider a soft biological shell shell in the state of dynamic equilibrium. It is supported by intraluminal pressure p = 20 kPa The strain distribution in the wall of the bioshell is shown in Fig. 1. The maximal elongation of the longitudinal muscle fibers, λ_l = 1.35, is observed in the cardio-fundal region along the *greater* curvature of the organ. A part of the fundus bordering the body experiences the maximal biaxial extension with λ_l = 1.35, λ_c = 1.04 in that area. The cardia and the body of the stomach along the *lesser* curvature, both undergo biaxial deformation with λ_l = 1.01, λ_c = 1.24, while the antrum-pyloric region along the *greater* curvature is under uniaxial strain, λ_l = 0.5, λ_c = 1.16. Negative circumferential deformations are registered in the cardia and the pylorus. Thus, the fundus and the body of the organ undergo biaxial distension and the cardia and antrum-pyloric areas are subjects to uniaxial elongation.

Analysis of the total force distribution in the bioshell demonstrates that maxT_l = 9.3 mN/cm, T_c = 14.5 mN/cm are recorded in the fundus and the body. The maximum T_c = 34.7 mN/cm is registered in a small area of the body along the *lesser* curvature of the stomach. In the antrum and the lower cardia, total forces of average intensity T_l = 4.1

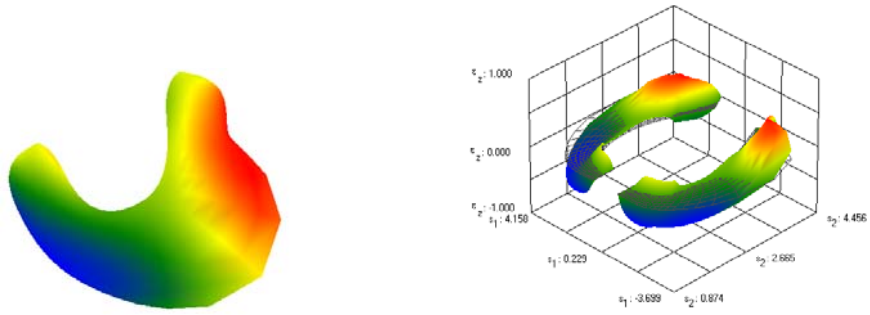

Longitudinal deformation

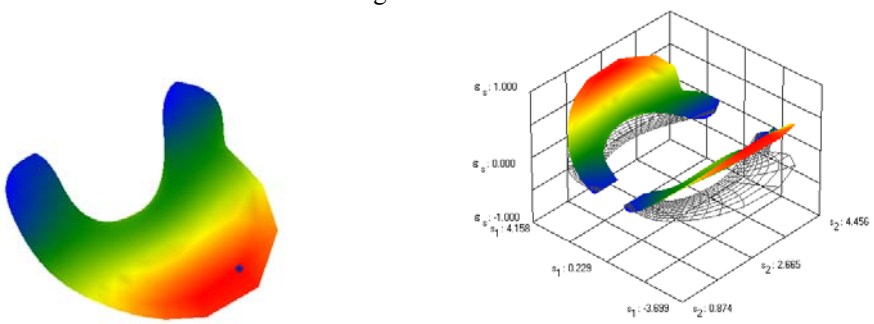

Circumferential deformation

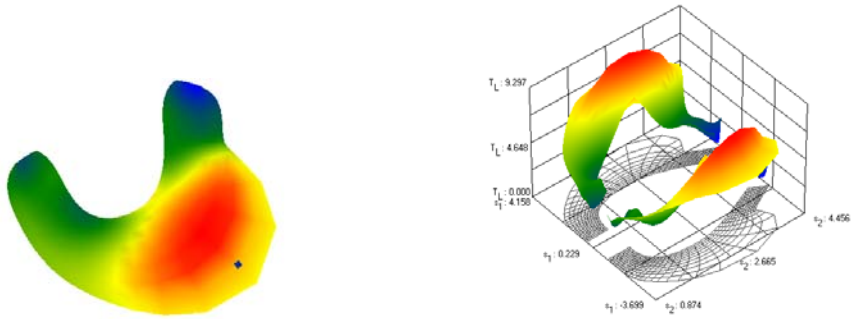

Total force in the longitudinal syncytium

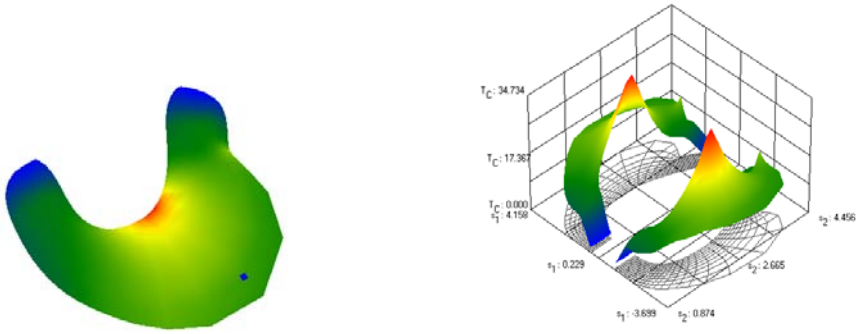

Total force in the circumferential syncytium

Figure 1: Static distribution of deformations and total forces in the longitudinal and circumferential smooth muscle syncytia of the inflated human stomach. Hereafter, results of simulations are presented on the entire stomach and the open surface envelope, respectively.

mN/cm, T_c = 14.5 mN/cm are observed. Again, in the pylorus and the cardia the total force in the circumferential direction equals zero, while in the longitudinal direction, T_l = 3.0 mN/cm. The proximal part of the cardia remains unstressed with $T_l = T_c = 0$.

5.2 Electromechanical wave activity

Consider a case of two identical pacemaker cells located on the longitudinal and circular smooth muscle layers in the upper body along the greater curvature of the stomach. Let the cells discharge simultaneously multiple impulses (n = 5). The activation of ion channels on the membrane of muscle causes the generation of the waves of depolarization of amplitude $\varphi_{(l,c)}$ = 65 – 70 mV (Fig. 2). The velocity of the propagation of excitation varies between the syncytia and regions of the organ. Thus the wave φ_l quickly spreads within the longitudinal muscle fibers to encase a narrow zone within the anterior surface of the organ (t = 0.8 s). The wave φ_l sustains short wave-length and a constant amplitude 18 mV throughout 2.0 < t < 5.6 s. The high level of depolarization is observed in the pyloric region where φ_l = 25.2 mV is registered.

The propagation of the wave φ_c within the isotropic circular smooth muscle layer is faster compared to φ_l. Thus, at t = 0.8 s nearly a half of the anterior and posterior surfaces of the bioshell undergo even depolarization, 60 < φ_c < 66.5 (mV). The excitation quickly extends towards the lesser curvature. The cardiac and pyloric regions experience extensive depolarization with a maxφ_c = 63.3 mV. At t = 5.6 s the longitudinal and circular smooth muscle syncytia of the stomach show a similar pattern in the distribution of depolarization with the average amplitude $\varphi_l \approx$ 3.7mV, $\varphi_c \approx$ 7.5mV.

There is a smooth distribution of active forces of contraction in the fundus and the body of the stomach where T^a_l = 6.1 mN/cm and T^a_c = 7.4 mN/cm are generated during 0 < $t \leq$ 5.0 (s). The cardia and the antrum-pyloric regions generate less intense forces, T^a_l = 3.0 – 3.6 mN/cm and T^a_c = 3.7 – 4.4 mN/cm. At t = 5.6 s of the dynamic process the redistribution in stresses occurs with the high level of contraction, maxT^a_l = 7.9 mN/cm, seen in the body of the organ. There is a concentration in active force development in the circular smooth muscle layer in the body along its *lesser* curvature with maxT^a_c = 10.5 mN/cm. The rest of the fundus and the body experience even contractions, T^a_l = 6.9, T^a_c = 8.4 (mN/cm).

The pattern of total force distribution is similar to that observed at the state of dynamic equilibrium. There is an increase in the intensity of forces, which is consistent with the generation of active forces of contraction by the syncytia. Thus, maxT_l = 15.1 mN/cm, T_c = 22.4 mN/cm are seen in the body, and T_l = 2.7 mN/cm, T_c = 5.3 mN/cm in the cardia and the pylorus of the stomach.

6 DISCUSSION AND CONCLUSION

The main hurdle that every computational modeler faces during the development of a biomechanical model of a living object is the paucity of reliable information about mechanical characteristics of biological tissues. Until now, there have been only a few correctly planned and executed experimental studies that are dedicated to the analysis of the human stomach from the quantitative mechanical perspective. Results of investigations revealed that: 1) the wall of the stomach, like other soft tissues, exhibits nonlinear transversely anisotropic mechanical properties. The experimentally obtained data on force - ratio of elongation served as a basis for the construction of phenomenological constitutive relations. They successfully described and offered robust estimates of the mechanical behavior of the stomach. Recent studies by different research groups performed on cadaveric, surgically removed human stomachs and

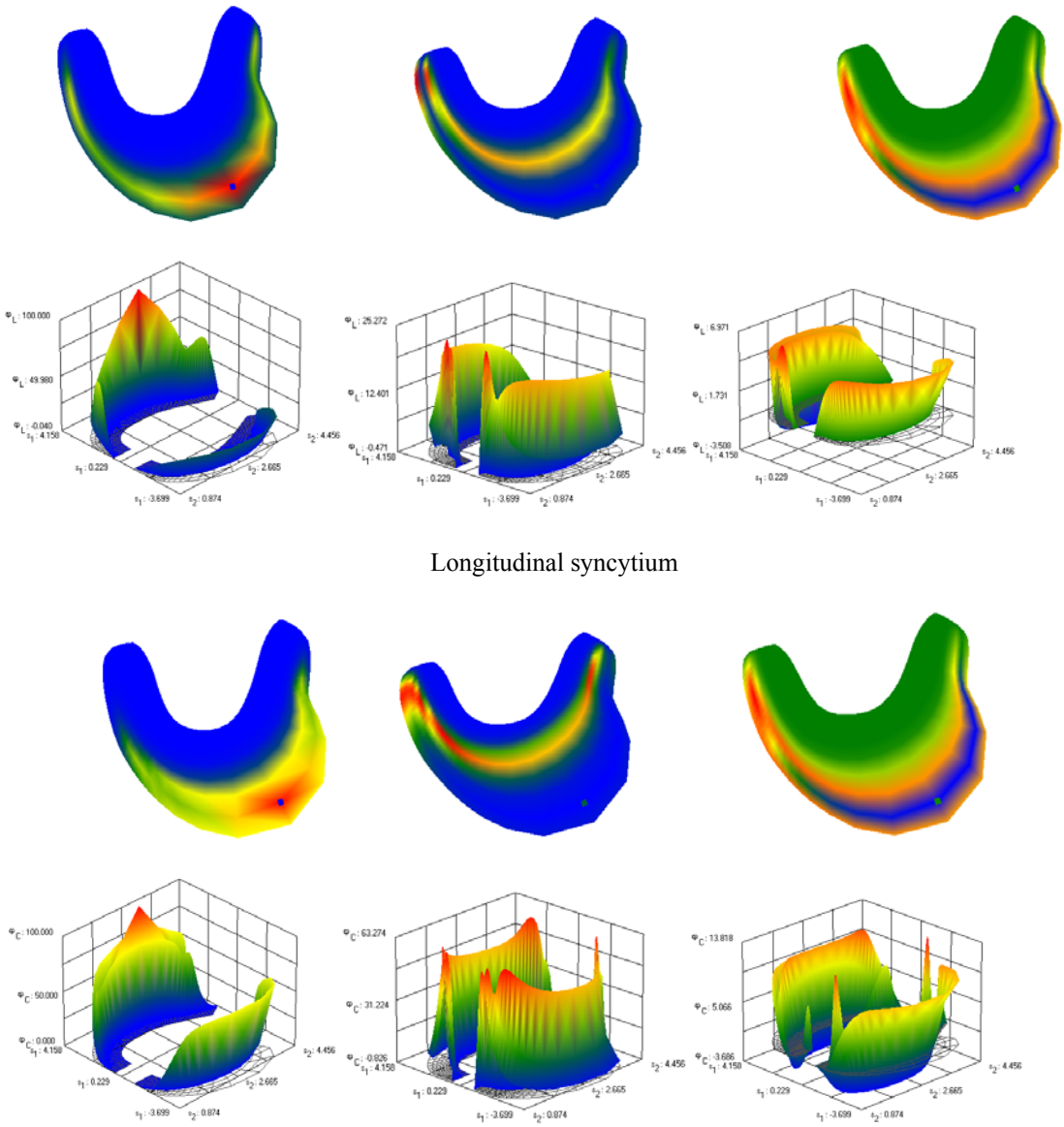

Longitudinal syncytium

Circumferential syncytium

$t = 0.8$ s $t = 2.0$ s $t = 5.6$ s

Figure 2: Dynamics of the propagation of the electrical wave of depolarization within different layers of the human stomach wall as a response to high frequency discharges of the pacemaker cell located in the body of the organ along its *greater* curvature.

healthy volunteers confirmed nonlinear anisotropic mechanical properties of the tissue and their regional dependence [16].

The presented model is an extension of the previous model [17]. It incorporates myoelectrical properties of the longitudinal and circular smooth muscle syncytia along with mechanical nonlinearity of the wall of the stomach. Special emphasis in the study was given to the questions of electromechanical coupling in smooth muscle syncytia and cable electromechanical wave activity.

Gastric motility is a result of electromechanical coupling that occurs at the cellular level and is manifested in the form of electromechanical wave activity within the organ wall. In the current study we restricted our attention to the cable, rather than to more general oscillatory, properties of smooth muscle syncytia. Even with these constructive

simplifications, the model reproduced and predicted: 1) patterns of the propagation of the wave of excitation within the electrically anisotropic longitudinal and electrically isotropic circular smooth muscle syncytia; 2) small isolated contraction waves in the two smooth muscle syncytia and nonpropagating tonic simultaneous contractions of both muscle layers superimposed on small contractions; 3) the development of wrinkles in the cardia, the body along the lesser curvature and the pylorus, and 4) high levels of tension in the body of the stomach along the lesser curvature.

A note of caution though should be made at this point of discussion. Care should be taken in transferring the results of simulations to explain real biomechanics of the human stomach. One has to bear in mind that the biological plausibility of the model is constrained by the model assumptions, despite the fact that the theoretical results resemble qualitatively patterns of electrical and mechanical activity that are observed in mainly animal studies *in vivo* and *in vitro*. At the moment there is no direct affirmative experimental evidence obtained on human subjects to run a detailed quantitative evaluation and comparison of the computational data. The proposed model of the human stomach as a soft biological shell can serve as a starting point for further expansions and biological improvements.

REFERENCES

[1] R.N. Miftakhov, Applications of the theory of soft thin shells in problems of biomechanics. *Biomech.: Probl. Invest.,* **Vol. VI**, pp. 51-56 (1988)

[2] A. Pullan, L. Cheng, R. Yassi and M. Buist, Modelling gastrointestinal bioelectric activity. *Prog. Biophys. Mol. Biol.* **85**, pp. 523-550 (2004)

[3] L. Cheng, R. Komuro, T.M. Austin, M.L. Buist and A. J. Pullan, Anatomically realistic multiscale models of normal and abnormal gastrointestinal electrical activity. *World J. Gastroenter.* **7**, pp. 1378-1383 (2007)

[4] A. Corrias and M.L. Buist, A quantitative model of gastric smooth muscle cellular activation. *Ann. Biomed. Eng.* **35**, pp. 1595–1607 (2007)

[5] A. Pal, J. Brasseur and B. Abrahamsson, A stomach road or « Magenstrasse » for gastric emptying. *J. Biomech.* **40**, pp. 1202–1210 (2007)

[6] A. Pal, K. Indireshkumar, W. Schwizer, B. Abrahamsson, M. Fried and J. G. Brasseur, Gastric flow and mixing studied using computer simulation. *Proc. R. Soc. Ser.* B **271**, pp. 2587–2594 (2004)

[7] R. Miftahof, H.G. Nam, and D. L. Wingate, Mathematical Modeling and Simulation in Enteric Neurobiology, *World Scientific Publ*. (2009)

[8] H. Suzuki, Cellular mechanisms of myogenic activity in gastric smooth muscle. *Jap. J. Physiol.* **50**, pp. 289-301 (2000)

[9] D.G.S. Hirst and H. Suzuki, Involvement of interstitial cells of Cajal in the control of smooth muscle excitability. *J. Physiol.* **576**, pp. 651-652 (2006)

[10] S.D. Koh, S.M. Ward, O. Tamas, K.M. Sanders and B. Horowitz, Conductances responsible for slow wave generation and propagation in interstitial cells of Cajal. *Curr. Opin. Pharmac.* **3**, pp. 579–582 (2003)

[11] G.L. Lyford, P.R. Strege, A. Shepard, Y. Ou, L. Ermilov, S.M. Miller, S.J. Gibbons, J.L. Rae, J.H. Szurszewski and G. Farrugia, Alpha 1C (Cav1.2) L-type calcium channel mediates mechanosensitive calcium regulation. *Am. J. Physiol.* **283**, pp. C1001-C1008 (2002)

[12] G.L. Lyford and G. Farrugia, Ion channels in gastrointestinal smooth muscle and interstitial cells of Cajal. *Curr. Opin. Pharmacol.* **3**, pp. 583-587 (2003)

[13] R. N. Miftakhov, Investigation of the human stomach tissue in uniaxial loading. *Hydroelast. Shells.* pp.163-171 (1983) (in Russian)
[14] R.N. Miftakhov, Experimental investigation of the stomach tissue in biaxial loading. *Invest Theor. Plates and Shells.* **Vol. XVIII**, pt. I, pp. 35-46 (1985) (in Russian)
[15] R.N. Miftakhov, Experimental investigations of the stomach under complex loading. *Hydroelast. Shells,* pp. 172-181 (1983) (in Russian)
[16] V. I. Egorov, I.V. Schastlivtsev, E. V. Prut, A. O. Baranov, and R.A. Turusov, Mechanical properties of the human gastrointestinal tract, *J. Biomech.* **35,** pp. 1417–1425 (2002)
[17] R.N. Miftakhov, *Experimental and Numerical Investigations of Soft Shells.* Ph.D. Thesis, Kazan State University, Russia, (1983) (in Russian).